

Photochemical Water Splitting by Bismuth Chalcogenide Topological Insulators

Catherine R. Rajamathi,^[a] Uttam Gupta,^[b] Koushik Pal,^[b] Nitesh Kumar,^[a] Hao Yang,^[a] Yan Sun,^[a] Chandra Shekhar,^[a] Binghai Yan,^[a] Stuart Parkin,^[c] Umesh V. Waghmare,^[b] Claudia Felser,^{*[a]} and C. N. R. Rao^{*[b]}

As one of the major areas of interest in catalysis revolves around 2D materials based on molybdenum sulfide, we have examined the catalytic properties of bismuth selenides and tellurides, which are among the first chalcogenides to be proven as topological insulators (TIs). We find significant photochemical H₂ evolution activity with these TIs as catalysts. H₂ evolution increases drastically in nanosheets of Bi₂Te₃ compared to single crystals. First-principles calculations show that due to the topology, surface states participate and promote the hydrogen evolution.

Layered-chalcogenide materials have recently exhibited robust catalysis for the hydrogen evolution reaction (HER).^[1] Bismuth-based layered chalcogenides, which are topological insulators, can probably be good catalysts for hydrogen evolution reaction. Topological materials are insulating in bulk with metallic surface states.^[2] As the contamination of catalyst surface is one of the problems in rendering it inactive, we believe that topological materials can help overcome this problem because of their protected surface states. The metallic surface states usually exhibit a Dirac-cone-type energy dispersion and are robust against surface defects, being protected by time reversal symmetry as shown in Figure 1. On the surface, the electron spin is in lock-up state with the momentum due to intrinsic interaction, the spin-orbit coupling (SOC) forming a vortex-like spin texture. Consequently, the forward- and backward-moving states carry opposite spin polarization and cannot be scattered into each other. Since backscattering is forbidden, the topological surface states are expected to be ideal conducting channels for electron transport. Photochemical catalysis on similar

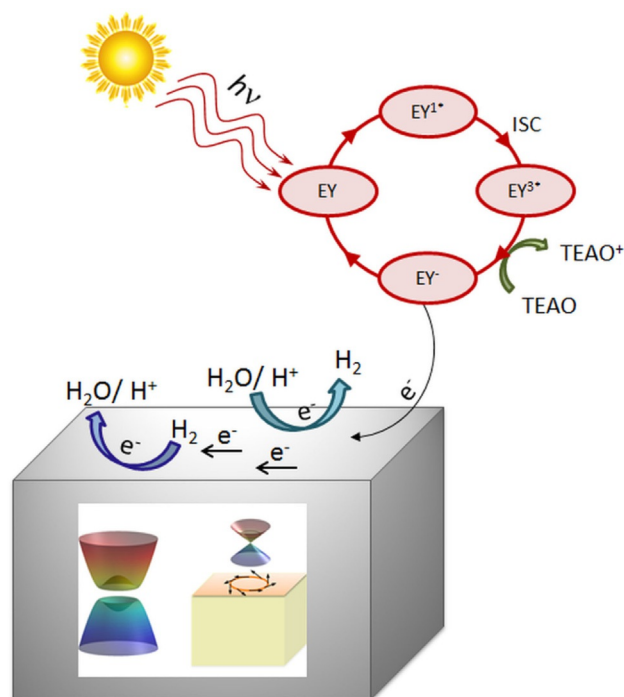


Figure 1. Schematic representation of the surface states of topological insulators and of the photocatalytic splitting of water on a topological insulator.

topological materials, Weyl semimetals (WSM) have been discussed by us recently.^[3]

Topological surface states of TIs exhibit robust transport against scattering and against environmental perturbations. The first feature promises fast and low-dissipation electron transport channels with high mobility, which may improve the conductivity of electrodes in electrochemical reactions. The second feature serves stable supply of itinerant electrons at the interface, which may serve as a robust electron bath^[4] for the charge transfer for the chemical reaction. Therefore, we expect that topological states may demonstrate interesting catalytic properties. The question still remains whether the spin polarized topological states can interfere with the catalytic process directly. We have explored photocatalysis by topological insulators in the light of the recent reports that metallic 1T-MoS₂ and 1T-MoSe₂ exhibit excellent performance in generating H₂ from H₂O by the dye-sensitized photochemical process.^[5] Conventional layered catalytic materials such as 2H-MoS₂ yields H₂ from water on sensitization with a dye but the metallic 1T-MoS₂ is far superior yielding about 600 times more hydrogen than 2H-MoS₂.^[5a] Similar results are found with 1T-

[a] C. R. Rajamathi, Dr. N. Kumar, H. Yang, Y. Sun, Dr. C. Shekhar, B. Yan, Dr. C. Felser
Max Planck Institute for Chemical Physics of Solids
01187 Dresden (Germany)
E-mail: felser@cpfs.mpg.de

[b] U. Gupta, K. Pal, Dr. U. V. Waghmare, Prof. C. N. R. Rao
Chemistry and Physics Materials Unit
Theoretical Sciences Unit, International Centre for Materials Science
and Sheik Saqr Laboratory, Jawaharlal Nehru Centre for
Advanced Scientific Research, Jakkur P. O.
Bangalore 560064 (India)
E-mail: cnrrao@jncasr.ac.in

[c] Dr. S. Parkin
Max Planck Institute for Microstructure Physics
06120 Halle (Saale) (Germany)

Supporting Information for this article can be found under:
<https://doi.org/10.1002/cphc.201700344>.

MoSe₂.^[4b] The metallic surface along the basal planes of 1T-MoS₂ is catalytically active along with the edges, the metallicity of the basal planes determining the hydrogen evolution reaction (HER) activity and the stability of the catalyst.^[6] In this article, we discuss the experimental results on photochemical water splitting by topological insulators such as Bi₂Te₃, M₂X₃ (X=Se and Te) compounds where M=metal and X=chalcogenide have a quintuple layered structure where the interlayers are held together by weak van der Waals forces. Taking Bi₂Te₃ as the base compound, we have substituted both anions and cations independently to obtain other topologically non-trivial compounds such as Bi₂Te₂Se, Bi₂Se₃ and topologically trivial Sb₂Te₂Se. The sample was characterized and synthesis details have been highlighted in the Experimental Section and Supporting Information. The single crystals were characterized using XRD as shown in Figure S1. Nanosheets of Bi₂Te₃ were characterized using XRD, TEM and FESEM (Figure S2–3 and S6a). The band gap of the single crystals and nanosheets of Bi₂Te₃ was ≈ 0.35 eV as calculated from diffuse reflectance spectroscopy (Figure S4). We have investigated dye-sensitized photocatalytic hydrogen generation of all these compositions. We have carried out first-principles calculations to understand the catalytic activity of these novel materials.

On absorption of light, the Eosin Y (EY) dye goes to the singlet excited state EY^{1*}, which via efficient intersystem crossing goes to the low-lying EY^{3*} excited state. Using triethanolamine (TEAO) as the sacrificial agent, EY^{3*} is reduced to EY⁻ species.^[7] In the presence of hydrogen evolution site like WSMs and TIs the EY⁻ species transfer the electron to the surface of the catalyst leading to charge separation, thereby reducing water to hydrogen^[8] (Figure 1). Photocatalytic HER study was carried out with single crystals of Bi₂Te₃, Bi₂Se₃, Bi₂Se₂Te and Sb₂Te₂Se over a period of 6 hours.

The performance of the catalysts was measured as the activity per hour and the turnover frequency (TOF) in terms of the activity per unit weight and per mole of the catalyst, respectively. The hydrogen evolved after three hours in Bi₂Te₃ was 192 $\mu\text{mol g}^{-1}$ which increases to 627 $\mu\text{mol g}^{-1}$ on further addition of 14 μmol of dye after 3 hours shown in Figure 2. Hydrogen evolved after three hours in Bi₂Te₂Se was 152 $\mu\text{mol g}^{-1}$ which increases to 447 $\mu\text{mol g}^{-1}$ on further addition of dye

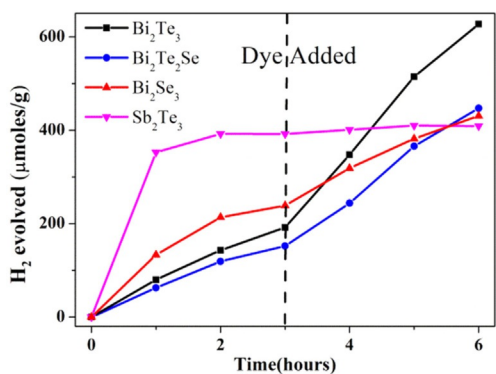


Figure 2. Catalytic behavior of the topological insulators under study. Bi₂Te₃ is the most active among the series.

(Figure 2). The hydrogen evolved after three hours in Sb₂Te₂Se was 395 $\mu\text{mol g}^{-1}$ which does not show noticeable increase on further addition of dye. The photocatalytic activity of Bi₂Te₃ and Bi₂Te₂Se was 72 and 60 $\mu\text{mol h}^{-1} \text{g}^{-1}$ with TOF of 0.06 and 0.045 h^{-1} and further increase to 161 and 107 $\mu\text{mol h}^{-1} \text{g}^{-1}$ with TOF of 0.13 and 0.08 h^{-1} (Figure 2). Sb₂Te₂Se a topologically trivial material does not exhibit good catalytic efficiency with a reasonable activity for an hour (196 $\mu\text{mol h}^{-1} \text{g}^{-1}$) and TOF of 0.11 h^{-1} with almost zero activity in the later 5 hours even on further addition of dye (Figure 2). We observed superior photocatalytic hydrogen evolution in Bi₂Se₃, but it was not as robust as Bi₂Te₃, decomposing in the reaction mixture during HER. The activity and TOF decreases from 161 and 107 $\mu\text{mol h}^{-1} \text{g}^{-1}$ and 0.13 and 0.08 h^{-1} respectively (Figure 2). We observe that the activities of Bi₂Te₃ and Bi₂Te₂Se are comparable but over a period of time the activity of selenium-substituted Bi₂Te₃ decreases significantly with respect to Bi₂Te₃. In Bi₂Te₂Se, the Se-sites are passivated over a period which leads to a decrease in the number of active sites, thereby decreasing the activity. Thus, the activity of Bi₂Te₂Se is lower relative to Bi₂Te₃ over long periods of observation. We also observe that the activity of Bi₂Se₃ decreases considerably due to passivation of the catalyst surface (Figure 2).

The Bi₂Te₃ nanosheets with surface area of 14.6 $\text{m}^2 \text{g}^{-1}$ (see nitrogen adsorption isotherm in Figure S5) was used for hydrogen evolution studies. The hydrogen evolved in Bi₂Te₃ nanosheets after 3 hours was 2018 $\mu\text{mol g}^{-1}$ which increases to 5521 $\mu\text{mol g}^{-1}$ after 6 hours, with no further addition of dye as shown in Figure 3. The activity of nanosheets is clearly better in comparison to single crystals due to the high surface area and greater number of active sites available for water reduction. Bi₂Te₃ crystals can be cycled for the hydrogen evolution whereas the activity of the nanosheets is noticeably lowered in the second cycle, not so remarkable and needs improvement as shown in Figure 4. The stability of Bi₂Te₃ was tested by soaking them in the reaction mixture for 24 h and performing EDX study before and after catalysis (Figure S6).

The steady-state absorption spectra of the dye recorded with and without catalyst is shown in Figure S7a. The topological surface can protect the electrons on the surface and assist

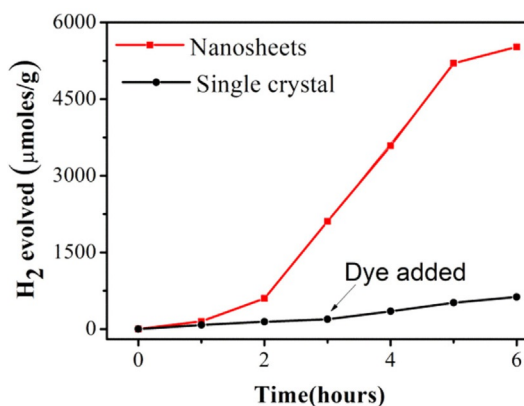


Figure 3. Comparison of HER activities of single crystals and nanosheets of Bi₂Te₃.

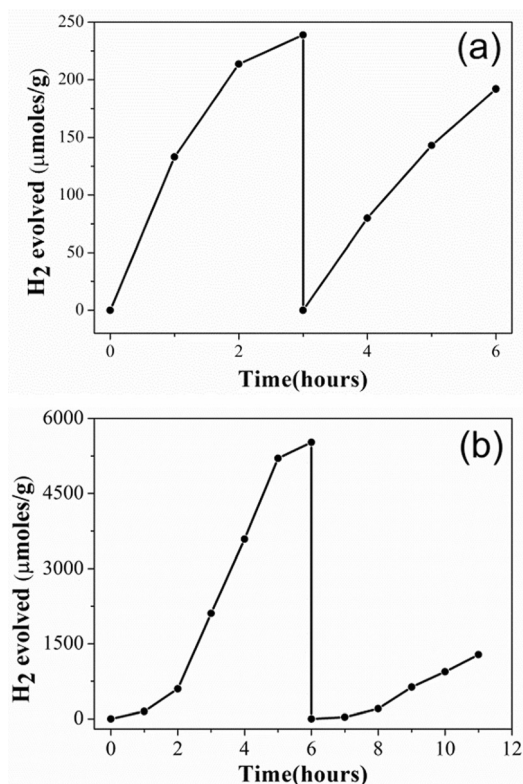


Figure 4. Cycling studies to check the stability of the: a) Bi₂Te₃ single crystals and b) nanosheets in solution. The activity of the Bi₂Te₃ nanosheets reduces drastically. The single crystals, however, are more robust in comparison.

the HER by increasing the life time of the excited electron. The following concept was probed by Transient absorption (TA) spectroscopy. The dye was taken in (15% v/v) triethanolamine solution and was excited at various wavelengths (480, 520, 560 and 600 nm) as shown in Figure S7 b. Maximum intensity was obtained at 560 nm. The catalyst was then added to the solution and was excited at 560 nm. Interestingly, we observe an increase in the intensity of the peak in the presence of the catalyst. The concentration of the catalyst was the same as it in

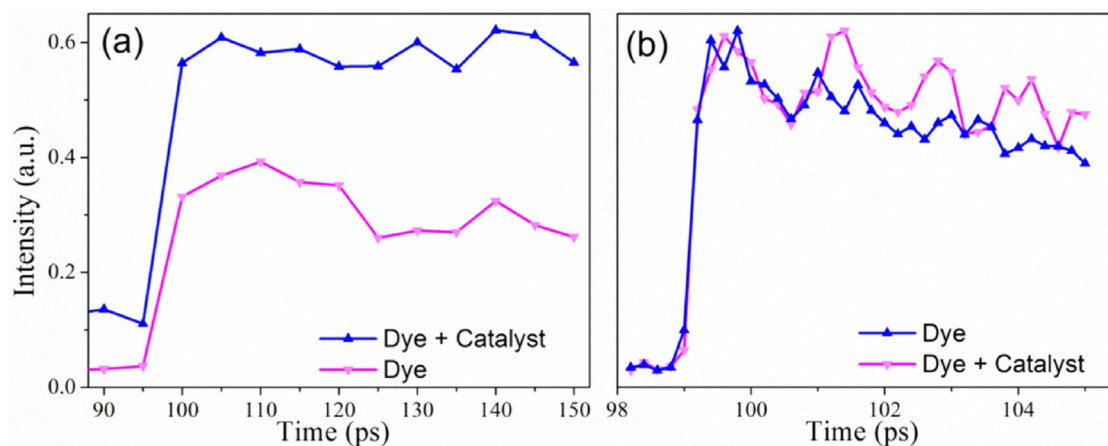


Figure 5. The comparison of transition absorption spectra of dye and catalyst in triethanolamine: a) at 5 ps pulse and b) 200 fs pulse.

the HER. The TA-curve indicates that the electrons on the surface of the catalyst stay for a longer time as compared to the dye (Figure 5a). TA spectra recorded at 200 fs time pulse for 5 ps clearly indicate that electron decay occurs immediately in the absence of the catalyst whereas in the presence of the catalyst the electron decay is much slower (Figure 5b). Therefore, electrons on the surface of the catalyst are protected from decaying faster.

Mott–Schottky analysis of the sample was done at the onset potential of the sample under the reaction conditions similar to those in photocatalytic hydrogen evolution. The dye is replaced by the electrochemical potential. The polarization curve is given in Figure S8 a. The frequency chosen for Mott–Schottky analysis was obtained from the frequency corresponding to phase angle change in the Bode plot (Figure S8 b). The Mott–Schottky curve shows that the charge carrier type is n-type with a donor density of $1.3 \times 10^{22} \text{ m}^{-3}$ for Bi₂Te₃ nanosheets. The flat band potential is estimated to be -0.36 V (vs. Ag/AgCl) as derived from Figure 6.

Bi₂Se₃ and Bi₂Te₃ are strong topological insulators (TIs)^[2b] in three dimensions (3D) with quintuple layers of their formula unit stacked along the z-direction. Nontrivial topology of the bulk electronic wavefunctions of a topological insulator manifests as the gapless topological states in the surface electronic

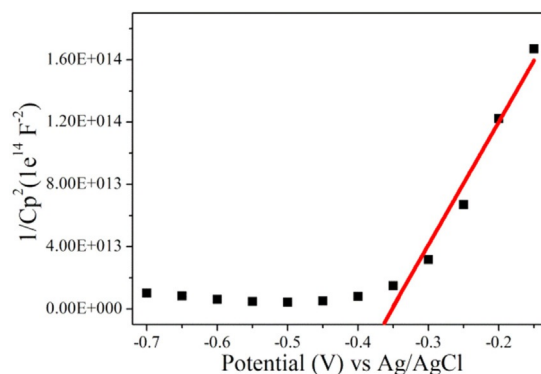


Figure 6. Mott–Schottky plot of Bi₂Te₃ nanosheets.

structure. In the slab geometry, Bi_2Se_3 and Bi_2Te_3 exhibit topological metallic states (Dirac cone appears at Γ point) when their slab unit cells contain 15 and 30 atomic layers, respectively (see Figures 7a,b).

Hence, to take the effect of topological surface states on the catalytic activity into account, we have performed calculations of Bi_2Se_3 and Bi_2Te_3 slabs containing 15 and 30 atomic layers, respectively. To assess the activity of these 3D TIs in the hydrogen evolution reaction, we have calculated work functions of these compounds with (001) surface orientation with Se or Te termination. The work functions of Bi_2Se_3 and Bi_2Te_3 calculated without the inclusion of van der Waals interaction are 5.51 eV and 4.89 eV respectively. The corresponding energies of the Fermi level (when the vacuum potential is set to 0 eV) of the slabs of Bi_2Se_3 and Bi_2Te_3 are at -5.51 eV and -4.89 eV, respectively. These values are clearly below the standard redox potential (-4.44 eV) of HER. Inclusion of van der Waals interaction and an increased thickness of the slab do not alter the values of the work functions of Bi_2Se_3 and Bi_2Te_3 significantly (see Table S1). Since, surface metallicity is two-dimensional in nature and is associated with a Dirac point, the corresponding density of states vanishes at the Fermi level.

To explain the observed photocatalytic activity of the Bi_2Se_3 family of topological insulators, we have determined the frequency-dependent optical dielectric tensor (i.e. optical absorption spectrum) of Bi_2Se_3 (see Figure 9a) and Bi_2Te_3 (Figure 9b) in their bulk as well as slab geometries. In Bi_2Se_3 , the topological surface states give rise to new infra-red (IR) peaks (marked

with blue arrows in Figure 9a) in the absorption spectrum. Looking at the electronic structure of the bulk (Figure 8a) and the surface (Figure 7a) of Bi_2Se_3 and the corresponding density of states (Figure 8b), it becomes clear that the electrons from the metallic surface states as well as from the bulk valence bands get photo-excited to the empty conduction bands. The strongest peak in the density of states of the conduction band (i.e. corresponding to the peak at 1.3 eV) has the highest population of photo-excited electrons. Comparing the peaks in the DOS in Figure 9b (see the blue dashed arrow) and absorption spectrum in Figure 9a (i.e. the peak corresponding to 1.7 eV), we confirm that the photo excitation of the electrons from the valence to this (1.7 eV) conduction band is quite feasible. Thus, the photoelectrons of Bi_2Se_3 populate states at $(-5.51 \text{ eV} + 1.3 \text{ eV}) = -4.21 \text{ eV}$ with respect to vacuum that lies just above the standard redox potential (-4.44 eV) of the HER. Thus, H^+ ions receive these photo-excited electrons from the conduction band at -4.2 eV and get reduced to H_2 . A similar mechanism holds for Bi_2Te_3 . The electronic structure of the bulk (Figure 8c), and the surface (Figure 7b) of Bi_2Te_3 and their DOS (Figure 7d) reveal that similar to Bi_2Se_3 , this material also facilitates transition of electrons from the metallic surface states and the bulk valence band to the empty conduction band in the bulk. Comparing Figure 8d and Figure 9a, we see that the photo-excited electrons largely populate the conduction band at 0.8 eV. Hence, the photo-electrons of Bi_2Te_3 are in the states at $(-4.89 \text{ eV} + 0.8 \text{ eV}) = -4.09 \text{ eV}$, which readily supplies electrons to H^+ ions for HER (at -4.44 eV). In Figure 10

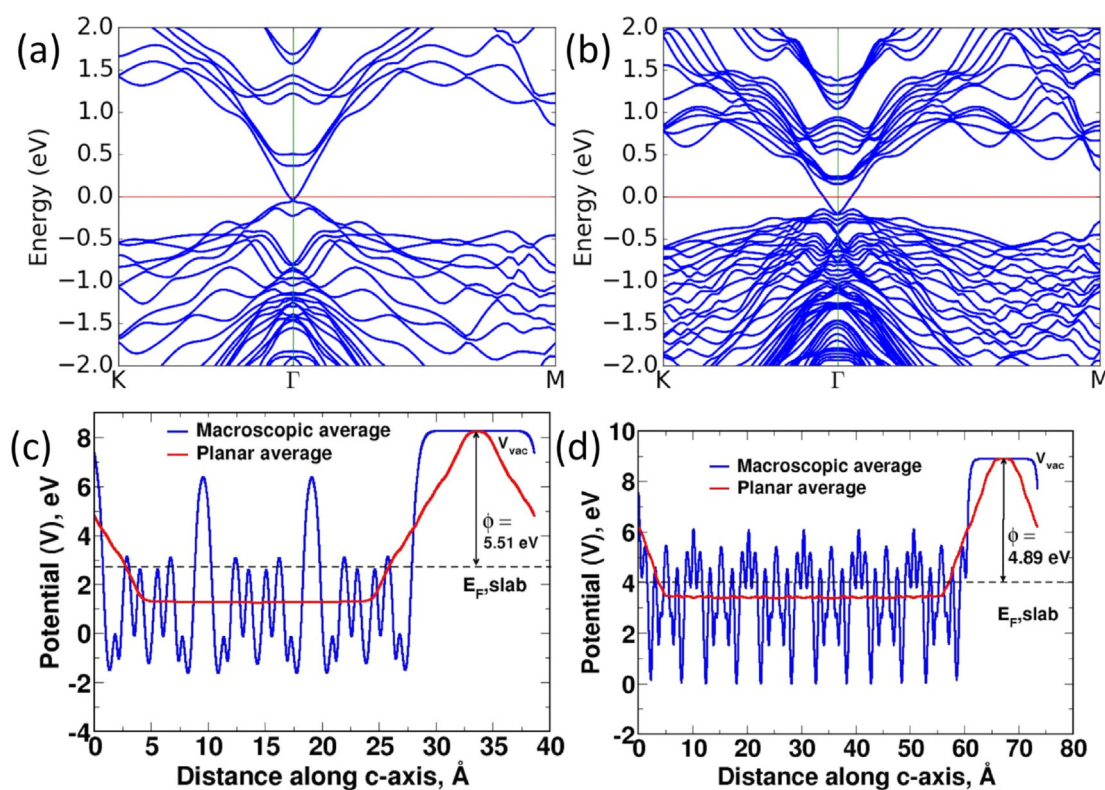


Figure 7. Electronic structures of the (001) surfaces of: a) Bi_2Se_3 and b) Bi_2Te_3 showing gapless Dirac cones at the Γ point. Planar and macroscopic average of the electrostatic potentials of: c) Bi_2Se_3 and d) Bi_2Te_3 slabs calculated as functions of distance along the c-axis of the unit cell (layered direction in their crystal structures). The estimates of work functions (ϕ) of Bi_2Se_3 and Bi_2Te_3 are 5.51 and 4.89 eV, respectively. V_{vac} is the vacuum potential energy.

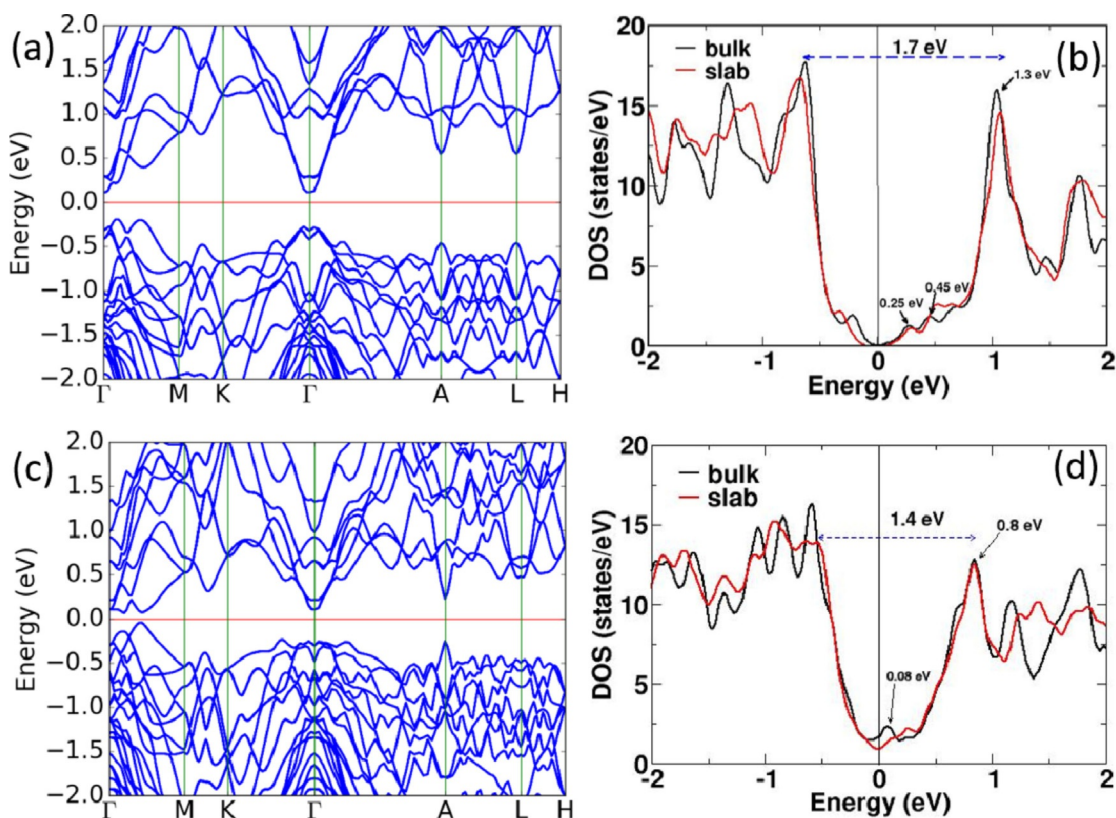


Figure 8. Electronic structures of the bulk: a) Bi_2Se_3 and c) Bi_2Te_3 . The density of states (DOS) for the bulk and slab unit cells of: b) Bi_2Se_3 and d) Bi_2Te_3 .

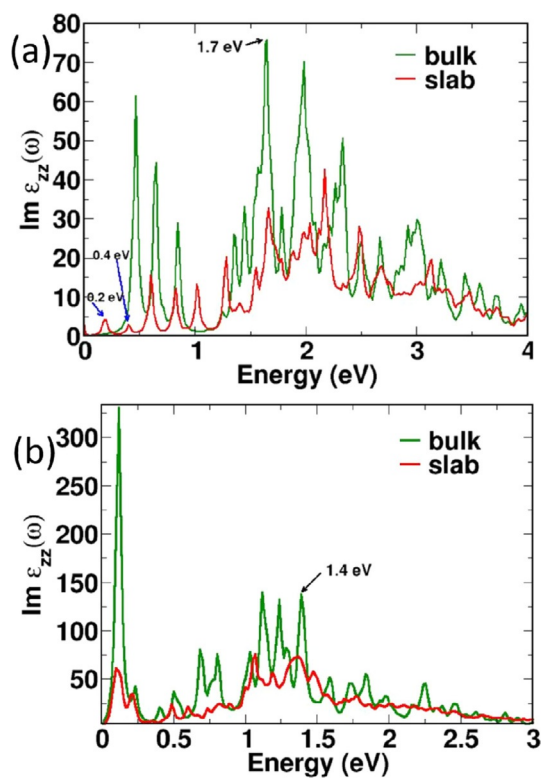


Figure 9. Frequency-dependent optical dielectric function for the bulk and slab unit cells of: a) Bi_2Se_3 and b) Bi_2Te_3 .

we present a schematic diagram for the density of states to explain the mechanism of photocatalysis in Bi_2Se_3 .

When light shines on this material, electrons from the surface and the bulk valence bands get excited to the conduction band and largely populate the bands associated with the strongest peak in DOS. This peak lies slightly above the redox potential of the hydrogen evolution reaction, and donates electrons to H^+ ions to produce H_2 . Due to their topology,

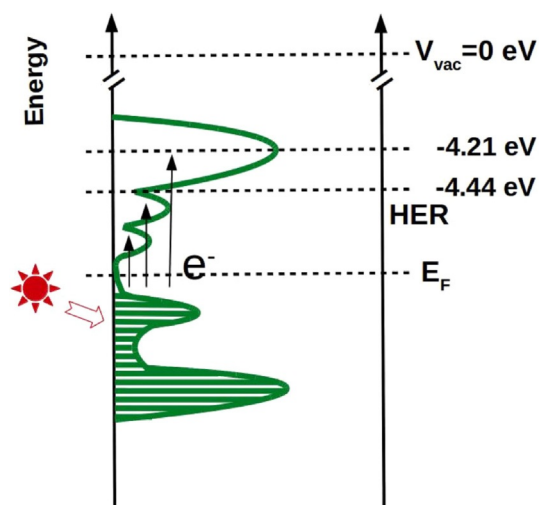


Figure 10. Schematic diagram of the density of states and mechanism for the photocatalytic activity of Bi_2Se_3 .

the parity of these bands is opposite, which permits optical transitions.

In conclusion, it is significant that bismuth chalcogenide-based topological insulators such as Bi_2Te_3 exhibit robust photocatalytic hydrogen evolution. The activity decreases with the substitution of Se in Te and increases in nanosheets. From theory, we find that the photo-catalytic activity of the topological insulators arises from the photoexcitation of the electrons from: a) bulk valence to the bulk conduction bands, and b) topological surface states to the conduction band of the bulk. We also find that the topological surface states give rise to new IR bands in the absorption spectra of these materials that slow down the decay of photoelectrons to lower energy states.

Experimental Section

Single crystals of Bi_2Te_3 , $\text{Bi}_2\text{Te}_2\text{Se}$ and $\text{Sb}_2\text{Te}_2\text{Se}$ were synthesized using the flux method. Nanosheets of Bi_2Te_3 were synthesized by a procedure in ref. [9]. Details of synthesis of the samples are provided in the Supporting Information. All the materials were characterized by powder X-ray diffraction using an image-plate Huber G670 Guinier camera with a Ge (111) monochromator and Cu K_α radiation. The X-ray diffraction patterns are shown in Figure S1. FESEM images were recorded using Nova Nano FESEM 600 FEI (see the Supporting Information). The surface area of the samples was determined using the BET technique.

Single crystals of topological insulators Bi_2Se_3 , Bi_2Te_3 , $\text{Bi}_2\text{Te}_2\text{Se}$ and $\text{Sb}_2\text{Te}_2\text{Se}$ were dispersed in 48 mL of triethanolamine (15% v/v) aqueous solution with 14 μmol of Eosin Y dye and sonicated for 30 mins. The vessel was thoroughly purged with N_2 and was irradiated with 100 W halogen lamp with constant stirring. The evolved gases were manually collected from the headspace of the vessel and analyzed with a TCD detector in PerkinElmer Clarus ARNEL 580GC gas chromatograph.

Our first-principles calculations are based on density functional theory as implemented in the Quantum Espresso code^[10] which uses pseudopotentials to model the interaction between core and valence electrons. We used norm-conserving pseudopotentials generated^[11] from the solutions of fully relativistic Dirac equation for an atom to take into account the effect spin-orbit coupling in our calculations. Exchange-correlation energy of the electrons was treated within a generalized gradient approximated (GGA) functional as parametrized by Perdew, Burke and Ernzerhof.^[12] We truncated the plane-wave basis used in representation of the Kohn-Sham wavefunctions and charge density with cut-off energies of 60 Ry and 240 Ry, respectively. Discontinuity in the occupation numbers of the electrons at the Fermi level were smeared with a broadening of $k_B T = 0.003$ Ry in the Fermi-Dirac function. We determined work functions of Bi_2Se_3 and Bi_2Te_3 from calculations on their slabs with (001) surface orientation taking 15 and 30 atomic layers, respectively. While constructing the periodic cell with a slab, we used optimized atomic coordinates of the bulk at their experimental lattice structures,^[13] and included a vacuum of length 10 Å along the c-direction to keep the interaction between the periodic images of the slab low. We estimated the work function (Φ)^[14] by taking the difference between the constant potential in the vacuum (V_{vac}) and the Fermi energy of the slab ($E_{\text{F,slab}}$), that is, $\Phi = V_{\text{vac}} - E_{\text{F,slab}}$. We find that the effect of van der Waals interactions (at the level of Grimme dispersion correction (DFT-D2)^[15]) on the calcu-

lated work functions is not significant (see Table S1 in the Supporting Information). Hence, we present here the results of calculations that do not include van der Waals interaction. To study the optical absorption spectra, we obtained the frequency dependent dielectric tensor of both these compounds in their bulk as well as slab forms taking into account the effect of spin-orbit coupling. We used uniform grid of $9 \times 9 \times 1$ k-points in our calculations on the slab.

Acknowledgements

This work was financially supported by ERC Advanced Grant No. 291472 "Idea Heusler". We thank Michael Rajamathi for providing nano samples of Bi_2Te_3 and Bi_2Se_3 for the study. We thank Prof. Anshu Pandey and Guru Pratheep for their help in TA studies and Manjeet Chettri for Mott-Schottky measurements.

Conflict of interest

The authors declare no conflict of interest.

Keywords: bismuth · first-principles calculations · hydrogen evolution · photochemical water splitting · topological insulators

- [1] a) S. Zhuo, Y. Xu, W. Zhao, J. Zhang, B. Zhang, *Angew. Chem. Int. Ed.* **2013**, *52*, 8602–8606; *Angew. Chem.* **2013**, *125*, 8764–8768; b) X. Hai, W. Zhou, K. Chang, H. Pang, H. Liu, L. Shi, F. Ichihara, J. Ye, *J. Mater. Chem. A* **2017**, *5*, 8591–8598; c) Y. Huang, Y. Liu, D. Zhu, Y. Xina, B. Zhang, *J. Mater. Chem. A* **2016**, *4*, 13626–13635; d) Q. Lu, Y. Yu, Q. Ma, B. Chen, H. Zhang, *Adv. Mater.* **2016**, *28*, 1917–1933.
- [2] a) D. Ceresoli, T. Thonhauser, D. Vanderbilt, R. Resta, *Phys. Rev. B* **2006**, *74*, 024408; b) H. Zhang, C. X. Liu, X. L. Qi, X. Dai, Z. Fang, S. C. Zhang, *Nat. Phys.* **2009**, *5*, 438–442; c) M. Z. Hasan, C. L. Kane, *Rev. Mod. Phys.* **2010**, *82*, 3045–3067; d) X. L. Qi, S. C. Zhang, *Rev. Mod. Phys.* **2011**, *83*, 1057–1110.
- [3] C. R. Rajamathi, U. Gupta, N. Kumar, H. Yang, Y. Sun, V. Süß, C. Shekhar, M. Schmidt, B. Yan, S. Parkin, C. Felser, C. N. R. Rao, *Adv. Mater.* **2017**, DOI: 10.1002/adma.201606202.
- [4] a) D. Voiry, M. Salehi, R. Silva, T. Fujita, M. Chen, T. Asefa, V. B. Shenoy, G. Eda, M. Chhowalla, *Nano Lett.* **2013**, *13*, 6222–6227; b) J. Xiao, L. Kou, C.-Y. Yam, T. Frauenheim, B. Yan, *ACS Catal.* **2015**, *5*, 7063–7067.
- [5] a) U. Maitra, U. Gupta, M. De, R. Datta, A. Govindaraj, C. N. R. Rao, *Angew. Chem. Int. Ed.* **2013**, *52*, 13057–13061; *Angew. Chem.* **2013**, *125*, 13295–13299; b) U. Gupta, B. S. Naidu, U. Maitra, A. Singh, S. N. Shirodkar, U. V. Waghmare, C. N. R. Rao, *APL Mater.* **2014**, *2*, 092802.
- [6] C. Tsai, K. Chan, J. K. Nørskov, F. Abild-Pedersen, *Surf. Sci.* **2015**, *640*, 133–140.
- [7] S. Min, G. Lu, *J. Phys. Chem. C* **2012**, *116*, 25415–25424.
- [8] T. Lazarides, T. McCormick, P. Du, G. Luo, B. Lindley, R. Eisenberg, *J. Am. Chem. Soc.* **2009**, *131*, 9192–9194.
- [9] Y. Zhang, L. P. Hu, T. J. Zhu, J. Xie, X. B. Zhao, *Cryst. Growth Des.* **2013**, *13*, 645–651.
- [10] P. Giannozzi, et al., *J. Phys. Condensed Matter* **2009**, *21*, 395502.
- [11] A. Dal Corso, *Comput. Mater. Sci.* **2014**, *95*, 337–350.
- [12] J. P. Perdew, K. Burke, M. Ernzerhof, *Phys. Rev. Lett.* **1996**, *77*, 3865.
- [13] A. Belsky, et al., *Acta Crystallogr. Sect. B* **2002**, *58*, 364–369.
- [14] N. E. Singh-Miller, N. Marzari, *Phys. Rev. B* **2009**, *80*, 235407.
- [15] S. Grimme, *J. Comput. Chem.* **2006**, *27*, 1787–1799.

Manuscript received: April 1, 2017

Revised manuscript received: May 31, 2017

Accepted manuscript online: July 6, 2017

Version of record online: August 8, 2017